H. Zhong and X. Zeng,
S. Afr. J. Chem., 2008, **61**, 22–25,
<http://journals.sabinet.co.za/sajchem/>.

Preparation of MAl_2O_4: Eu^{2+}, Sm^{3+} (M = Ca, Sr, Ba) Phosphors by the Combustion Method and their Luminescent Properties

Hua Zhong[a,b]* and Xirui Zeng[a,b]

[a]*Provincial Key Laboratory of Coordination Chemistry, Jinggangshan University, Jian, 343009, People's Republic of China.*

[b]*College of Chemistry and Chemical Engineering, Jinggangshan University, Jian, 343009, People's Republic of China.*

Received 24 February 2006; revised 15 October 2007; accepted 24 October 2007.

ABSTRACT

A series of MAl_2O_4: Eu^{2+}, Sm^{3+} (M = Ca, Sr, Ba) phosphors was prepared by the combustion method, and the influence of these alkaline earth metals on the structure and luminescent performances for these phosphors was investigated. A relationship was established between their composition, crystallization capacity and luminescent properties. The results show that the $CaAl_2O_4$: Eu^{2+}, Sm^{3+} and $SrAl_2O_4$: Eu^{2+}, Sm^{3+} phosphors exhibit monoclinic crystal systems and that the $BaAl_2O_4$: Eu^{2+}, Sm^{3+} phosphor exhibits a hexagonal structure. The alkaline earth metal has a positive effect on the crystallization process, the heat treatment procedure and the luminescent properties of the corresponding phosphors. According to the order Ca > Sr > Ba, the maximum emission wavelengths of the corresponding phosphors are found at 505 nm, 490 nm and 478 nm, and the relevant colours of emitted light are between blue and green, which indicates that there is a clear blue shift in the emission spectra, but their excitation spectra show almost no difference. The decay curve shows that the afterglow intensity and time are not only related to the activating processes and the hole transport, but also to the phase structure and the grain size, which is in the order Sr > Ca > Ba.

KEYWORDS

Long afterglow, alkaline earth aluminates, spectra, combustion method.

1. Introduction

Due to the thermal stimulated recombination of holes and electrons at traps which leave holes or electrons in a long-lived excited state at room temperature, long-lasting phosphorescence in materials has attracted considerable attention.[1–6] The luminescence of Eu^{2+} is very strongly dependent on the host lattice, which can occur from the ultraviolet to the red region of the electromagnetic spectrum. It is well known that persistent luminescence is due to the trapping of energy in the defects, followed by a slow thermal bleaching of the traps and transport of the charge carriers and recombination with the Eu^{2+} ion, which results in its excitation and emission spectra usually being broad. Eu^{2+}-doped solids have been widely used as luminescent materials due to their excellent properties, such as high brightness, no radiation, long duration, excellent photoresistance and environmental application capability.[7–10] It is commonly accepted that the quality of a luminescent material is largely determined by the synthesis method. In previous reports, MAl_2O_4: Eu^{2+} (M = Ca, Sr, Ba) phosphors were mostly synthesized by high temperature solid-state and sol-gel methods, which require quite long reaction times at high temperatures, and always display large grain sizes, while the microwave heating technique was also used for preparing MAl_2O_4: Eu^{2+} phosphors.[11–16] In recent years, due to the combustion method displaying unique advantages of lower synthesis temperature, shorter synthesis time and controlled size of particles, it is a more recent and more reliable method for preparing long afterglow phosphor materials. Moreover, the alkaline earth metals have a positive influence on the crystallization process, the heat treatment procedure and the luminescent properties of the corresponding phosphors. The luminescence of Eu^{2+} has been widely studied but detailed investigation is limited and there have been very few reports on the luminescent properties of MAl_2O_4 (M = Ca, Sr, Ba) phosphors activated by two rare earth ions. Thus, in order to obtain better possible luminescent materials, it was important to search for a new method and study the relationship among preparation conditions, structure and luminescent performance. The purpose of the present study is therefore to establish a relationship between the powder formation conditions, crystallizing capacity and luminescent properties of MAl_2O_4 (M = Ca, Sr, Ba) phosphors activated by Eu^{2+} and Sm^{3+} ions, which were prepared by the combustion method at 600 °C. The structure, thermal process and luminescent properties of those samples were investigated and are reported.

* To whom correspondence should be addressed. E-mail address: hua_zh@163.com

2. Experimental

2.1. Sample Preparation

A series of MAl_2O_4: Eu^{2+}, Sm^{3+} (Eu^{2+}: 0.15 mol %, Sm^{3+}: 0.15 mol %) (M = Ca, Sr, Ba) phosphors was prepared by the combustion method and they were labelled as samples A (M = Ca), B (M = Sr) and C (M = Ba), respectively. In the synthesis, calcium, strontium and barium nitrates, aluminium hydroxide, boric acid (added as flux), nitric acid, urea (all of AR grade purity), europium oxide (99.99%) and samarium oxide (99.99%) were used as starting materials. The rare earth oxides were dissolved in nitric acid, and $M(NO_3)_2$, $Al(OH)_3$, $Eu(NO_3)_2$ and $Sm(NO_3)_3$ in the desired molar ratio were dissolved in a urea solution with constant stirring at 80 °C. After evaporation of water at 110 °C, the dark gels were combusted for a few minutes at 600 °C, which yielded the samples.

2.2. Sample Characterization

Phase analysis was performed by X-ray diffraction (D8/ADVANCE, Germany), with Cu K_α radiation. The step scans were taken over the range of 2θ angles from 20 to 70 °. For the evaluations of average crystal size of samples, the Scherrer equation (1) was used, where L denotes the average crystal size, λ the wavelength of the X-rays used (0.154 nm), β the effective line width of the reflection, and θ the Bragg angle.

$$L = 0.9\lambda/\beta \cos\theta \,. \quad (1)$$

Differential thermal and thermogravimetric analyses (DTA/TG-DTG) of the precursors were conducted on CRY-2P and WRT-2P thermal analysers. Sample masses were *ca*. 40 mg and thermal runs were performed in N_2 (99.99%) with a gas flow rate of 20 mL min^{-1}. The atmosphere was air and the temperature increased from 50 to 700 °C at a ramp rate of 10 °C min^{-1}. The platinum sample pot had a depth of 5 mm and contained alpha-alumina as reference material.

2.3. Optical Measurements

The emission and excitation spectra of the samples were obtained at room temperature using a Perkin-Elmer LS 55 luminescence spectrometer with a xenon flash lamp. The excitation and emission slits were set at 2.5 nm, and the excitation spectra were automatically corrected for the variation in the lamp intensity by a second photomultiplier and a beam-splitter. The emission spectra were corrected by dividing the measured emission intensity by the ratio of the observed spectrum of a calibrated tungsten lamp and its known spectrum from 300 to 900 nm. All of the spectra were measured at a scan speed of 1000 nm min^{-1}.

The decay curve of afterglow was measured at room temperature with an ST-86LA brightness meter, and the samples were irradiated by 365 nm light for 20 min. During the experiments, since the samples were comparatively stable, different control experiments showed good reproducibility, differing only by the equipment standard deviation.

3. Results and Discussion

To study the processes occurring in the course of gel heating, the thermal analysis results of DTG and DTA for the MAl_2O_4: Eu^{2+}, Sm^{3+} (M = Ca, Sr, Ba) precursors are shown in Figs 1 and 2, respectively. Fig. 1 also includes, as an inset, the TG curves. These changes of residual mass and temperature difference with temperature are shown with corresponding integral curves. As indicated in Fig. 1, there are three principal mass loss regions in the DTG curve for the three precursors with increase of temperature. The broadband peak with a T_{max} at about 130–150 °C is observed in all the DTG curves, and is assigned with a high degree of certainty to the dehydration of crystallized water in the initial precursor. After the dehydration is completed, the region of mass loss from 190 to 400 °C is attributed to the decomposition of the hydrocarbon (CH_x) and amino-group organic components. The significant mass loss region > 410 °C is attributed to the decomposition of carboxyl alkaline earth metal group and carboxyl aluminium groups. Furthermore, at temperatures up to 530 °C, no additional changes in the masses of the residues were recorded from the three precursors. On the other hand, as shown in Fig. 2, there are five principal endothermic peaks in the DTA curves for the precursors with increase in temperature. The deeper endothermic peak around 180 °C in the DTA curve, corresponding to the first weak mass loss shown by TG, is due to the dehydration of the precursors. The smooth endothermic peak at 200 °C and the small and shallow endothermic peaks at 250 °C are a result of the decomposition of $Al(OH)_3$ into AlO(OH) and the release of crystal water.[17] The large and sharp endothermic peak between 280 and 420 °C, accompanied by the major mass loss, corresponds to the dehydroxylation of the mixed hydroxides into oxides. The endothermic peak (*ca.* 510 °C) is a result of the decomposition and/or melting of nitrate. During this stage, amorphism M-Al-O: Eu^{2+}, Sm^{3+} (M = Ca, Sr, Ba) occurs. Above 540 °C, heat impact is not distinctive, which indicates that the complex has decomposed completely and changed gradually from the amorphous state to full crystal grains.

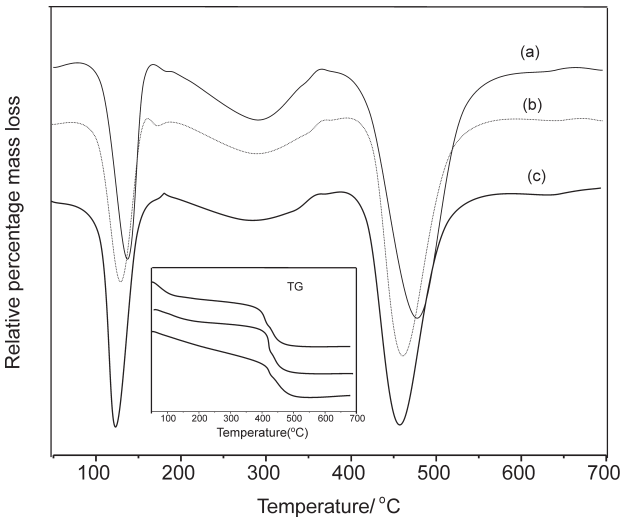

Figure 1 TG-DTG curves of the precursors: (**a**) $SrAl_2O_4$: Eu^{2+}, Sm^{3+}; (**b**) $CaAl_2O_4$: Eu^{2+}, Sm^{3+}; (**c**) $BaAl_2O_4$: Eu^{2+}, Sm^{3+}.

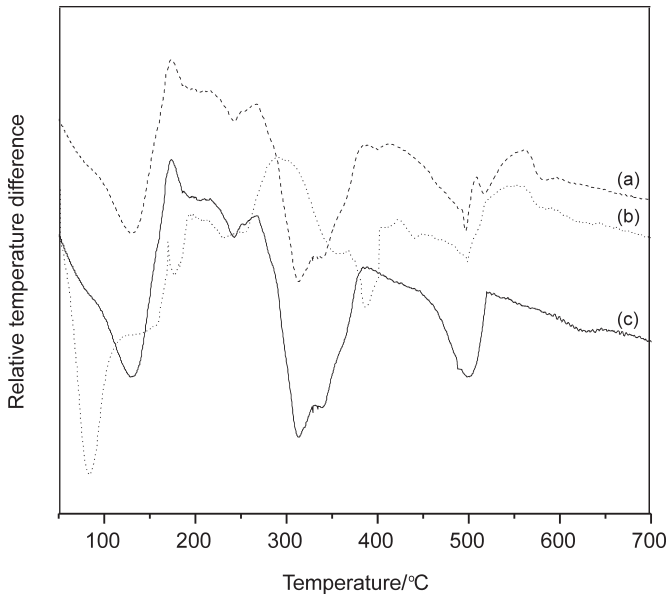

Figure 2 DTA curves of the precursors: (**a**) $SrAl_2O_4$: Eu^{2+}, Sm^{3+}; (**b**) $CaAl_2O_4$: Eu^{2+}, Sm^{3+}; (**c**) $BaAl_2O_4$: Eu^{2+}, Sm^{3+}.

The results shown by XRD reveal the influence of the alkaline earth metal on the crystallization of those phosphors. The d values and relative intensities (I/I_o) of the samples, as displayed in Fig. 3, correspond mainly to the reference values in JCPDS cards of MAl_2O_4 (M = Ca, Sr, Ba) No. 1-888, No. 34-0379 and No. 17-306, respectively, and the composition of the phosphors is in accordance with the desired molar ratio MAl_2O_4: Eu^{2+}, Sm^{3+}. At the same time, the results of the phase analysis obtained by XRD also

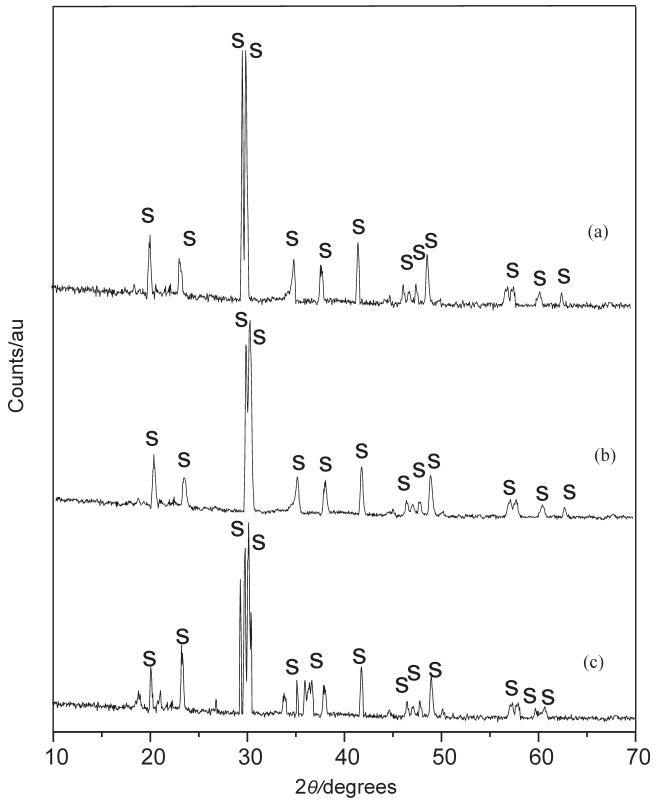

Figure 3 XRD patterns of the MAl_2O_4: Eu^{2+}, Sm^{3+} phosphors: (S) spinel; (**a**) $SrAl_2O_4$: Eu^{2+}, Sm^{3+}; (**b**) $CaAl_2O_4$: Eu^{2+}, Sm^{3+}; (**c**) $BaAl_2O_4$: Eu^{2+}, Sm^{3+}.

clearly show that most peaks are assigned to those of the MAl_2O_4 structure. Moreover, their structures change with change of M. Samples A and B exhibit monoclinic crystal systems and sample C a hexagonal structure. The doping Eu^{2+} and co-doping Sm^{3+} have very little influence on the structure of the luminescent materials, and a mixed compound of Eu^{2+} and Sm^{3+} is therefore not observed. The above analysis indicates that MAl_2O_4 crystalline phases can be formed at a relatively low temperature (600 °C) by the combustion method.

Table 1 reports the observed values of the lattice parameters and the evaluations of average crystal size of samples A, B and C. The values calculated reflect the trend of the crystallinity shown by the XRD patterns. A comparison of these samples shows that the particle size of the samples increases from 284 Å to 335 Å in the order B < A < C. This result reveals that the alkaline earth metal has a significant influence on the average crystal size. As is commonly accepted, the crystal size is one of the most important reasons for showing different luminescent properties, where smaller grain size is beneficial to the luminescent property.

Figs 4 and 5 illustrate the excitation and emission spectra of the three phosphors. As is well known, rare-earth phosphors may be separated into two types, i.e. broadband-emitting due to the transition between the 5d and 4f orbital gaps (Eu^{2+}, Ce^{3+}), or narrow line-emitting owing to the transition in the 4f levels

Table 1 Structure parameters of the MAl_2O_4: Eu^{2+}, Sm^{3+} (M = Ca, Sr, Ba) phosphors.

Sample	a/Å	b/Å	c/Å	V/Å^3	L/Å
A	8.745	8.251	5.183	374	307
B	8.429	8.903	5.211	391	284
C	8.661	8.326	5.257	379	335

a, b and c: cell parameters; V: crystal cell volume; L: average crystalline size.

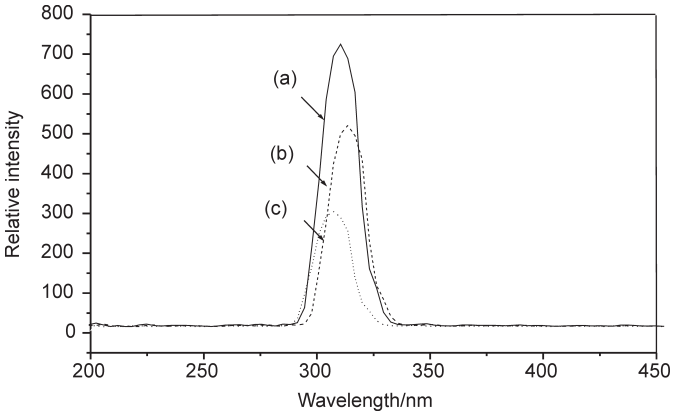

Figure 4 Excitation spectra of the MAl_2O_4: Eu^{2+}, Sm^{3+} phosphors: (**a**) $SrAl_2O_4$: Eu^{2+}, Sm^{3+}; (**b**) $CaAl_2O_4$: Eu^{2+}, Sm^{3+}; (**c**) $BaAl_2O_4$: Eu^{2+}, Sm^{3+}.

(Eu^{3+}, Tb^{3+}, Tm^{3+}). The excitation and emission spectra of the phosphors displayed in Figs 4 and 5 exhibit different shapes and broadband peaks in the photoluminescence spectra at room temperature. According to the order Ca > Sr > Ba, the maximum excitation wavelengths are observed at 321 nm, 316 nm and 312 nm, respectively. Moreover, the maximum emission wavelengths are found at 505 nm (M = Ca), 490 nm (M = Sr) and 478 nm (M = Ba), respectively, which corresponds to the colour of emitted light between blue and green. The emission spectra of these phosphors therefore shift blue light wavelength with the increase of ordinal number of the alkaline earth metals Ca, Sr and Ba, which can be due to the effect of crystal structure. Owing to the shielding of the electrons in the inner shell, the 4f electrons are not sensitive to lattice environment, but the 5d electrons may couple strongly to the lattice. Consequently, the mixed states of 4f5d will be split by the crystal field and will couple strongly to the lattice phonons, resulting in broadband absorption and emission. It is known that different host structures and crystallographic distortions will influence the crystal field environment of rare earth ions in the host structure.[18,19] For sample B, since the radii of Sr^{2+} and Eu^{2+} are very similar, there is no apparent effect of crystal structure when Sr^{2+} is partly substituted by Eu^{2+}. When Ca^{2+} or Ba^{2+} are partly substituted by Eu^{2+}, the phosphor displays a weak crystal microstrain and the action of crystal structure on Eu^{2+} is also different with a variation in the ionic radii. For sample A ($r_{Eu}^{2+} > r_{Ca}^{2+}$), the crystal will expand and the inter-repulsive force will be minimized, which results in an increase in

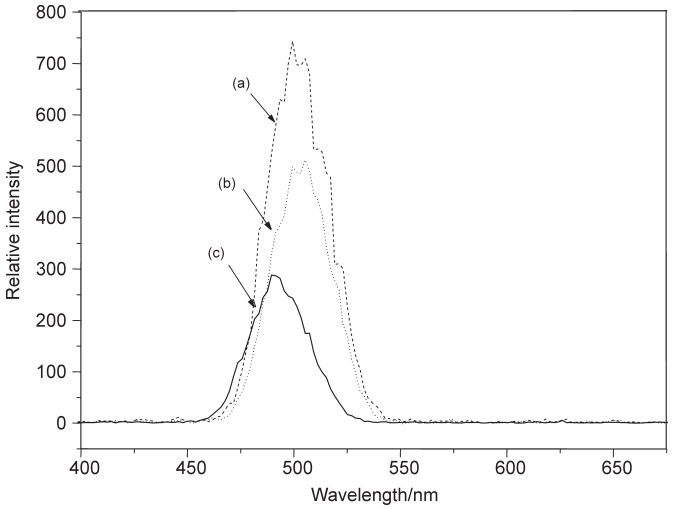

Figure 5 Emission spectra of the MAl_2O_4: Eu^{2+}, Sm^{3+} phosphors: (**a**) $SrAl_2O_4$: Eu^{2+}, Sm^{3+}; (**b**) $CaAl_2O_4$: Eu^{2+}, Sm^{3+}; (**c**) $BaAl_2O_4$: Eu^{2+}, Sm^{3+}.

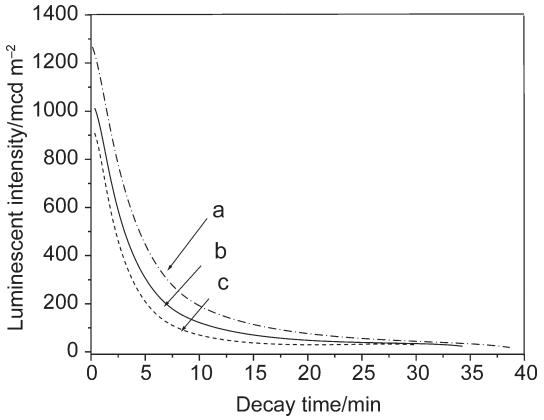

Figure 6 Afterglow curves of the MAl_2O_4: Eu^{2+}, Sm^{3+} phosphors: (**a**) $SrAl_2O_4$: Eu^{2+}, Sm^{3+}; (**b**) $CaAl_2O_4$: Eu^{2+}, Sm^{3+}; (**c**) $BaAl_2O_4$: Eu^{2+}, Sm^{3+}.

the emission wavelength. However, for sample C, the crystal will contract which results in a decrease in the emission wavelength.[20,21] With a decrease in crystal field strength, the luminescence of Eu^{2+} from different sublevels thus exhibits a clear blue shift.

The luminescent decay curves of the three phosphors, irradiated by 365 nm light for 20 min at room temperature, are shown in Fig. 6, which indicates that the afterglow decay tendency is described as follows: initial rapid decay, intermediate transitional decay and then a long-lasting phosphorescence. The initial rapid decay is due to the short survival time of an electron in Eu^{2+}, the intermediate transitional decay might be the capture of Eu^{2+} by a shallow trap energy centre and the very long-lasting decay could be attributed to the deep trap energy centre of Sm^{3+}.[22] As is well known, for the long persistent phosphorescence doping rare earth ions (Eu^{2+} and Sm^{3+}), Sm^{3+} could act as trap levels which capture the free holes, release the trapped holes and recombine with electrons, which accompanies the luminescence. In addition, the depth of trap level and the trap types will influence the emission lifetime.[23] Owing to the Sm^{3+} ions added as the auxiliary activator and partly substituting the alkaline earth metals M of MAl_2O_4, their energy levels have a relationship to the composition and structure of the host. For samples A and B, which display monoclinic crystal structures, the appropriate trap can be produced and afterglow phenomena can be observed. However, the shallow trap can be produced but the afterglow phenomenon is not markedly observed for sample C with the hexagonal crystal lattice.[21] In addition, with decreasing grain size, the surface energy should be increased dramatically, which attracts more vacancies.

The decay times of phosphors can be calculated using Eq. 2, where I is the phosphorescence intensity, A_1, A_2 and A_3 are constants, t is time, and τ_1, τ_2 and τ_3 are decay times for the exponential components, respectively.[24]

$$I = A_1 \exp(-t/\tau_1) + A_2 \exp(-t/\tau_2) + A_3 \exp(-t/\tau_3)\,. \qquad (2)$$

The values of the decay times for the three phosphors are shown in Table 2, and based on the above analysis, the sequence of afterglow intensity and time is in the order Sr > Ca > Ba.

4. Conclusion

A series of MAl_2O_4: Eu^{2+}, Sm^{3+} (M = Ca, Sr, Ba) phosphors was prepared by the combustion method at 600 °C, and characterized using X-ray powder diffraction and excitation and emission spectroscopy. Thermal analyses of these precursors were carried out. A relationship was established between the conditions of combustion synthesis, the crystallization capacities and the luminescent properties of the corresponding phosphors. There are three principal mass loss regions for the precursors in the DTG curve and five endothermic peaks in the DTA curves with an increase in temperature. Based on the XRD peaks, all phosphors are primarily identified as MAl_2O_4 phase, while samples A and B exhibit monoclinic crystal systems and sample C a hexagonal structure. The emission spectra of these phosphors shift towards the blue with the increase of ordinal number of the alkaline earth metals Ca, Sr and Ba. The order of afterglow intensity and decay time is Sr > Ca > Ba.

Table 2 Decay times of the MAl_2O_4: Eu^{2+}, Sm^{3+} (M = Ca, Sr, Ba) phosphors.

Sample	Initial intensity/mcd m^{-2}	Decay time/min		
		τ_1	τ_2	τ_3
A	1013	1.04	2.42	34.08
B	1257	1.08	2.64	37.11
C	915	0.97	2.13	30.56

Acknowledgements

This work was supported by the Science and Technology Bureau of Jian, Jiangxi Province of China (Project No. 20052817).

References

1 T. Matsuzawa, Y. Aoki, N. Takeuchi and Y. Murayama, *J. Electrochem. Soc.,* 1999, **143,** 2670–2675.
2 T. Aitasalo, P. Deren and H. Holsa, *J. Solid State Chem.,* 2003, **171**, 114–121.
3 L. Yuanhua, T. Zilong and Z. Zhongtai, *J. Eur. Ceram. Soc.,* 2003, **23**, 175–180.
4 K. Kato, I. Tsutai, T. Kamimura, F. Kaneko, K. Shinbo, M. Ohta and T. Kawakami, *J. Lumin.,* 1999, **82**, 213–220.
5 R. Sakai, T. Katsumata, S. Komuro and T. Morikawa, *J. Lumin.,* 1999, **85**, 149–154.
6 W. Jia, H. Yuan, S. Holmstrom, H. Liu and W.M. Yen, *J. Lumin.,* 1999, **83–84**, 465–469.
7 H. Liu, Y. Wang, J. Yang and W. Su, *J. Alloy Comp.,* 1993, **191**, 1–6.
8 S.H.M. Poort and G. Blasse, *J. Lumin.,* 1997, **72–74**, 247–253.
9 F.C. Palilla, A. K. Levine and M.R. Tomkus, *J. Electrochem. Soc.,* 1968, **115,** 642–647.
10 J.R. Qiu and K. Hirao, *Solid State Commun.,* 1998, **106**, 795–801.
11 T.L. Liu, D.X. Feng and P.H. Yang, *Rare Materials,* 2000, **19**, 297–302.
12 T. Katsumata, T. Nabae and K. Sasajima, *J. Amer. Ceram. Soc.,* 1998, **81**, 413–418.
13 Y. Murayama, Y. Aoki, N. Takeuchi and T. Matsuzawa, U.S. Patent No. 5424006 (1995).
14 H. Takasaki, S. Tanabe and T. Hanada, *J. Japan. Ceram. Soc.,* 1996, **104**, 322–327.
15 T. Katsumata, R. Sakai and S. Komuro, *J. Crystal Growth.,* 1999, **198–199**, 869–875.
16 M.D. Tang, C.K. Li and Z.W. Gao, *Chin. J. Lumin.,* 1995, **16**, 51–56.
17 K. Hayashi, S. Toyoda, H. Takebe and K. Morinaga, *J. Japan. Ceram. Soc.,* 1991, **99**, 550–556.
18 G. Blasse and A. Bril, *Philips Res. Rept.,* 1968, **23**, 201–207.
19 Y. Lin, Z. Zhang and Z. Tang, *Materials Chem. Phys.,* 2001, **70**, 156–161.
20 J. Geng and Z.P. Wu, *Materials Rev.,* 2002, **16**(5), 45–51.
21 Y.G. Chen, G.M. Qiu and Y.B. Sun, *J. Rare Earths,* 2002, **20**, 50–55.
22 T. Katasumata, T. Nabae and K. Sasajima, *J. Crystal Growth,* 1998, **183**, 361–367.
23 M. Ohta, M. Maruyama and T. Nishijo, *J. Japan. Ceram. Soc.,* 2000, **108**, 284–290.
24 T. Katsumata, T. Nabae and K. Sasajima, *J. Electrochem. Soc.,* 1997, **144**, L243.